How to cite: *Angew. Chem. Int. Ed.* **2021**, *60*, 9301 – 9305
International Edition: doi.org/10.1002/anie.202015769
German Edition: doi.org/10.1002/ange.202015769

Molybdenum Sulfide Clusters

Zeolite-Stabilized Di- and Tetranuclear Molybdenum Sulfide Clusters Form Stable Catalytic Hydrogenation Sites

Roland Weindl[+], Rachit Khare[+], Libor Kovarik, Andreas Jentys, Karsten Reuter, Hui Shi, and Johannes A. Lercher**

Abstract: *Supercages of faujasite (FAU)-type zeolites serve as a robust scaffold for stabilizing dinuclear (Mo_2S_4) and tetranuclear (Mo_4S_4) molybdenum sulfide clusters. The FAU-encaged Mo_4S_4 clusters have a distorted cubane structure similar to the FeMo-cofactor in nitrogenase. Both clusters possess unpaired electrons on Mo atoms. Additionally, they show identical catalytic activity per sulfide cluster. Their catalytic activity is stable (> 150 h) for ethene hydrogenation, while layered MoS_2 structures deactivate significantly under the same reaction conditions.*

Sulfide-based enzymes and the success of transition metal sulfide (TMS) catalysts for hydrotreating reactions have spurred wide interests to understand their activity and selectivity and especially the impact of the cluster size and structure for reductive catalysis. For the nitrogenase family, three TMS clusters have been identified acting as catalytically active sites, i.e., a Fe_4S_4 tetramer, the P-cluster (Fe_8S_7) and a third cluster Fe_7MS_9C (M = Fe, Mo, V); the Mo form, the so-called FeMo-cofactor, is the most intensively studied one among the Fe_7MS_9C family of clusters.[1]

The structures of the active site in the layered TMS materials have been equally well investigated compared to those in enzyme-based catalysts. In addition to the use of the former as hydrogenation and hydro-defunctionalization catalysts for hydrotreating of refinery fractions and renewable feedstocks,[2] TMS have recently drawn major interest as cathode materials in electrocatalysis.[3] Despite their similar chemical compositions, the TMS clusters in enzymes are well-defined entities, whereas TMS phases in industrial catalysts for hydrotreating predominantly form significantly larger slab-like structures.[4]

To achieve greater catalytic efficiencies, enzyme TMS clusters served as inspirations for the synthesis of active hydrogenation sites.[1e,5] Most of the prior studies focused on multi-step syntheses of TMS clusters and on using them as homogeneous organometallic catalysts in liquid phase.[6] A one-step synthesis could, in contrast, enable the use of such entities as potentially robust highly efficient catalysts. In this context, zeolites represent a promising group of porous supports that provide a stable and well-defined steric environment for the TMS clusters, mimicking partly the pockets of enzymes that host the active center.

Among the methods reported for immobilizing Mo and NiMo sulfide clusters on/in zeolites, ion exchange proves useful yet requires intricate synthesis of the cationic clusters.[7] Even worse, the groups of Tatsumi and Breysse reported that the zeolite-confined TMS clusters decomposed into MoS_2 slabs under reaction conditions.[7a,b] This structural degradation is likely caused by the presence of water after ion exchange.[8]

Using leads from Okamoto et al.,[9] we used chemical vapor deposition (CVD) and subsequent thermal treatments in reactive gases to incorporate homotopic size- and structure-selective Mo_xS_y clusters into the pores of zeolite NaY. The (uniformity of the) geometric structure and the spin state of the Mo_xS_y clusters were acquired in the present study by combining X-ray absorption spectroscopy (XAS), X-ray emission spectroscopy (XES), electron paramagnetic resonance (EPR) spectroscopy, and density functional theory (DFT) calculations. A close similarity was revealed between the tetranuclear Mo_4S_4 cluster and the Mo site in nitrogenase enzymes. These NaY-encaged Mo_xS_y clusters displayed outstanding stability for ethene hydrogenation, much superior to that of a traditional slab-MoS_2 catalyst.

$Mo(CO)_6$ encapsulated in a NaY zeolite was treated in H_2S/H_2 at 673 K for 2 h to form Mo_xS_y species within the zeolite (Mo_xS_y/NaY-sulf). The zeolite used was almost free of extra-framework Al (EFAl) and remained so after loading Mo and sulfidation (Figure S1). This catalyst was subsequently reduced in pure H_2 (Mo_xS_y/NaY-red) at 673 K for 2 h. Figure 1 shows the k^3-weighted extended X-ray absorption

[*] R. Weindl,[+] Dr. R. Khare,[+] Prof. A. Jentys, Prof. K. Reuter, Prof. J. A. Lercher
Department of Chemistry and Catalysis Research Center
Technical University of Munich
85747 Garching (Germany)
E-mail: Johannes.lercher@ch.tum.de
Dr. L. Kovarik, Prof. J. A. Lercher
Institute for Integrated Catalysis
Pacific Northwest National Laboratory
Richland, WA 99352 (USA)
Prof. K. Reuter
Fritz Haber Institute of the Max Planck Society
14195 Berlin (Germany)
Prof. H. Shi
School of Chemistry and Chemical Engineering, Yangzhou University
Yangzhou, Jiangsu, 225009 (China)
E-mail: shihui@yzu.edu.cn
[+] These authors contributed equally to this work.
Supporting information and the ORCID identification number(s) for the author(s) of this article can be found under: https://doi.org/10.1002/anie.202015769.

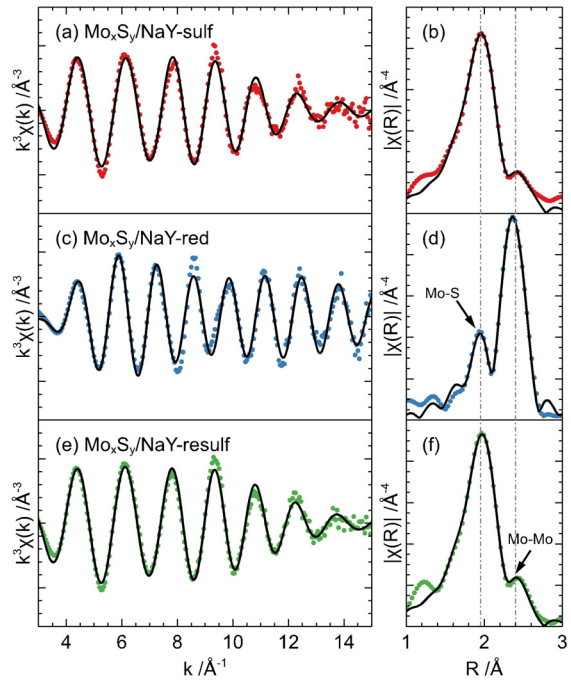

Figure 1. k^3-weighted EXAFS and FT EXAFS of Mo_xS_y/NaY-sulf (a,b), Mo_xS_y/NaY-red (c,d), and Mo_xS_y/NaY-resulf (e,f) catalysts. Experimental data is shown as closed symbols and the corresponding fits are shown as solid lines.

fine structure (EXAFS) and Fourier-transformed (FT) EXAFS of these catalysts at Mo K-edge. The corresponding fitted parameters are reported in Table 1. For Mo_xS_y/NaY-sulf, the Mo-S and Mo-Mo coordination numbers (CN) and interatomic distances (d) together with the S/Mo ratio of ≈ 2 (determined by elemental analysis) point to the overall cluster composition of Mo_2S_4. We hypothesize that in this structure, each Mo atom is coordinated to two bridging S atoms and one terminal S atom (either in *cis* or in *trans* configuration), resulting in theoretical $CN_{Mo\text{-}Mo} \approx 1$ and $CN_{Mo\text{-}S} \approx 3$. Slightly higher measured coordination numbers ($CN_{Mo\text{-}Mo} \approx 3.9$; $CN_{Mo\text{-}S} \approx 1.3$) are attributed to a minor presence of higher nuclearity species (e.g., a few MoS_2 slabs on the external surface of the zeolite). For Mo_xS_y/NaY-red, the observed $CN_{Mo\text{-}Mo}$ and $CN_{Mo\text{-}S}$ together with the S/Mo ratio of ≈ 1 suggest the reduced state to be a Mo_4S_4 cluster. Additionally, based on similar values of $d_{Mo\text{-}Mo}$ and $d_{Mo\text{-}S}$, we hypothesize the Mo_4S_4 cluster to resemble a distorted Mo_4-tetrahedron with an S atom sitting on each face. The composition and structure of this reduced state is different from a previously proposed Mo_4S_6 cluster with a cubane-like structure.[9] Instead, we propose that the deduced structure has a close similarity with the $MoFe_3S_3C$ subunit of the nitrogenase FeMo-cofactor (Table 1). The Mo_xS_y/NaY-red catalyst was resulfided in H_2S/H_2 at 673 K for 2 h to form Mo_xS_y/NaY-resulf. The observed Mo-Mo and Mo-S CN and interatomic distances in Mo_xS_y/NaY-resulf were similar to those in Mo_xS_y/NaY-sulf, suggesting that the transformation between the sulfided and reduced structures is reversible by switching between pure H_2 and H_2S/H_2 (Figure 3).[9]

Energy dispersive X-ray spectroscopy (EDS) mapping shows an even distribution of Mo across the zeolite particles (Figure S2), proving that Mo and S are not enriched at the outer surface of the crystallites. This indicates that Mo is initially evenly distributed and remains locally anchored as sulfide clusters with two different nuclearities. The decrease in zeolite micropore volume with increasing Mo loading also supports this conclusion (Figure S3). The absence of any larger particles in the high-angle-annular dark field-transmission electron microscopy (HAADF-TEM; Figure S2) showed further that the di- and tetranuclear clusters are the predominant, if not the only, form of Mo_xS_y. X-ray diffraction patterns of the Mo_xS_y-containing samples and the parent NaY zeolite show a change in the relative intensities of several diffraction peaks (Figure S4), attributed to a redistribution of Na^+ cations within the zeolite.[10] This indicates a slight preference of the location of the TMS clusters, requiring, however, additional analysis.

The hypothesized structures of Mo_2S_4 and Mo_4S_4 clusters were optimized using DFT and the results were compared against the experimental data (EXAFS). Interestingly, variations in the number of unpaired electrons in the Mo d-orbitals correlated with the Mo−Mo bond distances, while the Mo-S interatomic distances were insensitive to these changes (Figure 2).

The DFT-computed $d_{Mo\text{-}Mo}$ (Table S3) obtained for the thermodynamically most stable configurations (spin-multiplicity of 3 for Mo_2S_4 and 5 for Mo_4S_4) match excellently with the values obtained from EXAFS (Table 1). The computed $d_{Mo\text{-}S}$ however appear to be significantly lower than those observed experimentally, which we attribute to the fact that geometry optimization was performed in gas phase, while for

Table 1: EXAFS fitting parameters: coordination numbers (CN), interatomic distances (d), E_0, ΔE_0, and Debye–Waller factors (σ^2), for Mo–Mo and Mo–S paths in Mo_xS_y/NaY-sulf/red catalysts. $CN_{Mo\text{-}Fe}$, $CN_{Mo\text{-}S}$, $d_{Mo\text{-}Fe}$ and $d_{Mo\text{-}S}$ of the nitrogenase FeMo-cofactor are added for comparison.

	Path	CN	d [Å]	E_0 [eV]	ΔE_0 [eV]	$\sigma^2 \times 1000$ [Å^2]	R-factor
Mo_xS_y/NaY-sulf	Mo–S	3.9 ± 0.8	2.42 ± 0.01	19997	0.1 ± 2.4	6.6 ± 1.5	0.027
	Mo–Mo	1.3 ± 1.1	2.77 ± 0.03			10.3 ± 8.6	
Mo_xS_y/NaY-red	Mo–S	2.6 ± 1.4	2.47 ± 0.05	19995	0.4 ± 5.0	5.5 ± 5.0	0.039
	Mo–Mo	3.3 ± 2.0	2.66 ± 0.03			6.3 ± 2.6	
Mo_xS_y/NaY-resulf	Mo–S	4.1 ± 0.7	2.42 ± 0.01	19997	0.2 ± 2.1	6.4 ± 1.3	0.023
	Mo–Mo	1.0 ± 1.2	2.76 ± 0.03			8.2 ± 6.7	
Nitrogenase	Mo–S	3[a,b]	2.34[a], 2.32[b]				
FeMo-cofactor	Mo–Fe	3[a,b]	2.70[a], 2.61[b]				

[a] Data from ref. [1g]. [b] Data from ref. [1f].

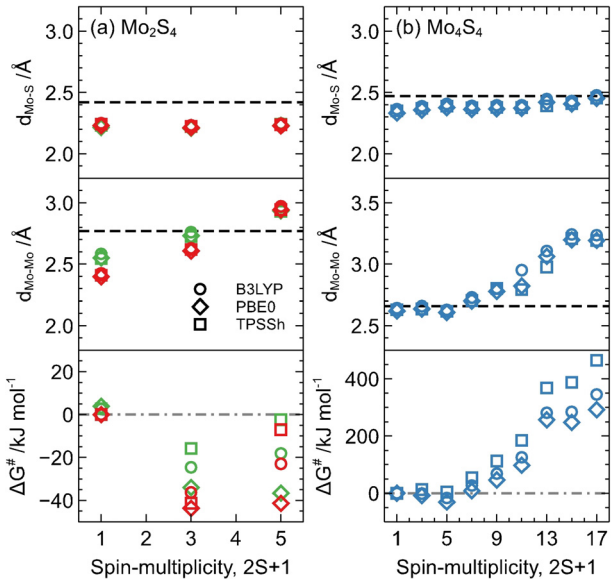

Figure 2. Average Mo–S (d_{Mo-S}) and Mo–Mo (d_{Mo-Mo}) interatomic distances, as well as the relative Gibbs free energies at 473 K ($\Delta G^{\#}$) of Mo_2S_4 (left) in *cis* (red) and *trans* (green) configurations, and Mo_4S_4 (right) clusters as a function of spin-multiplicity as calculated by DFT using B3LYP, PBE0, and TPSSh functionals. Experimentally observed d_{Mo-Mo} and d_{Mo-S} estimated from the EXAFS of Mo_xS_y/NaY-sulf/red catalysts are shown as dashed lines.

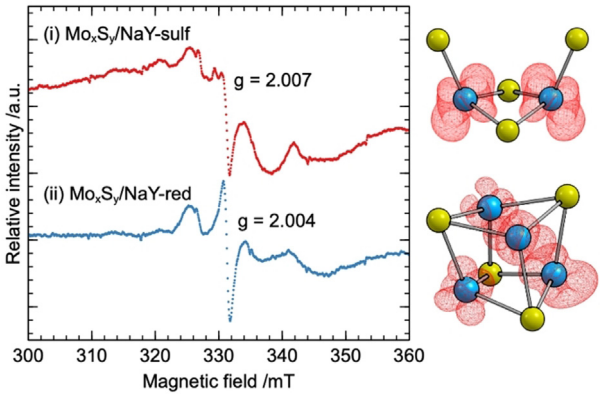

Figure 4. EPR spectra of Mo_xS_y/NaY-sulf/red catalysts (left) and the isosurface (0.02 a.u.) of the difference in alpha and beta electron densities (right) illustrating the location of unpaired electrons on *cis*-Mo_2S_4 (spin-multiplicity = 3) and Mo_4S_4 (spin-multiplicity = 5) clusters computed using DFT(B3LYP).

the zeolite-encaged clusters, the terminal S atoms are likely to interact with sodium cations in the zeolite, which is expected to elongate the bonds. As these interactions could also lead to charge transfer to/from clusters, we investigated the influence of positive/negative charge on the optimized geometries (Figure S5). The calculations indicate that the structural parameters of these clusters are influenced more by the spin-multiplicity than by the net charge on the clusters. Based on computed Gibbs free energies (Figure 2 and Tables S1 and S2), the lowest-energy structures have a spin-multiplicity of 3 (two unpaired electrons) and 5 (four unpaired electrons) for Mo_2S_4 and Mo_4S_4 (Figure 3), respectively. For Mo_2S_4, the *cis* configuration was found to be more stable and is further examined.

As DFT calculations correspond to one unpaired electron per Mo for both clusters, the presence of unpaired electrons on Mo was also deduced from the EPR measurements (Figure 4 left). The EPR spectra show an intense central line with g-values ≈ 2, in close agreement with the g-values

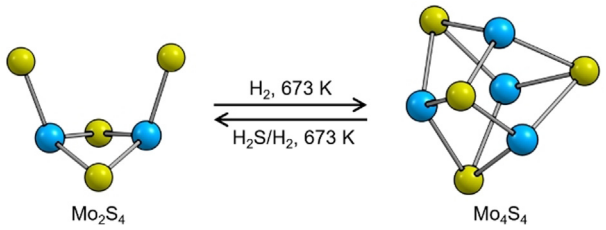

Figure 3. DFT-optimized Mo_2S_4 (*cis*) and Mo_4S_4 clusters. The depicted clusters were optimized with spin-multiplicity of 3 for Mo_2S_4 and 5 for Mo_4S_4 using B3LYP. Varying the functional did not result in a significant change in cluster geometry (Figure S6). S: yellow, Mo: blue.

reported for unpaired electrons in Mo species of different formal oxidation states in nitrogenase, nitrate reductase, and sulfur-bridged Mo dimer clusters.[11] Although EPR signals with $g \approx 2$ are commonly assigned to $S = {}^1/_2$ systems, these signals may also be interpreted as $M_s \pm 1$ transitions of systems with higher spin-multiplicities, e.g., *cis*-Mo_2S_4 (spin-multiplicity = 3) and Mo_4S_4 (spin-multiplicity = 5), with a large zero field splitting.[11a] Due to the lack of spin quantification, an in-depth electronic spin analysis of Mo_xS_y clusters proposed in this work is presently not achievable. It must also be noted that a mixture of clusters with different spin-multiplicities may be present as the DFT-computed Gibbs free energy difference between systems with slightly different multiplicities is relatively small (Figure 2 and Table S1 and S2).

The DFT calculations unambiguously support our finding that the unpaired electrons are indeed located on the Mo atoms of both Mo_xS_y clusters (Figure 4, right and Figure S6). In this regard, it is important to note that ionic clusters would result in formal Mo oxidation states of $+4/+2$ (assuming neutral Mo_2S_4/Mo_4S_4 clusters) which could not possess single unpaired electrons due to their even number of total valence electrons. However, the Mo–S bonds in these nanoclusters are likely to be covalent in character, which is supported by Hirshfeld/Mulliken population analysis and Mayer bond orders computed using DFT (Tables S4 and S5).

Further confirmation of the hypothesized structures of NaY encapsulated Mo_xS_y clusters was deduced from Mo Kα high energy resolution fluorescence detected X-ray absorption near edge structure (HERFD-XANES) and Mo Kβ valence-to-core (VtC) XES. The VtC XES spectra of Mo_xS_y/NaY-sulf/red catalysts are in close agreement with the simulated spectra of the optimized Mo_2S_4 and Mo_4S_4 structures (Figure S7 and Table S6) validating the structures suggested in this work. In addition, HERFD-XANES shows a shift towards lower absorption energies for the reduced catalyst supporting the proposed reduction of Mo centers in a pure H_2 atmosphere (Figure S10).

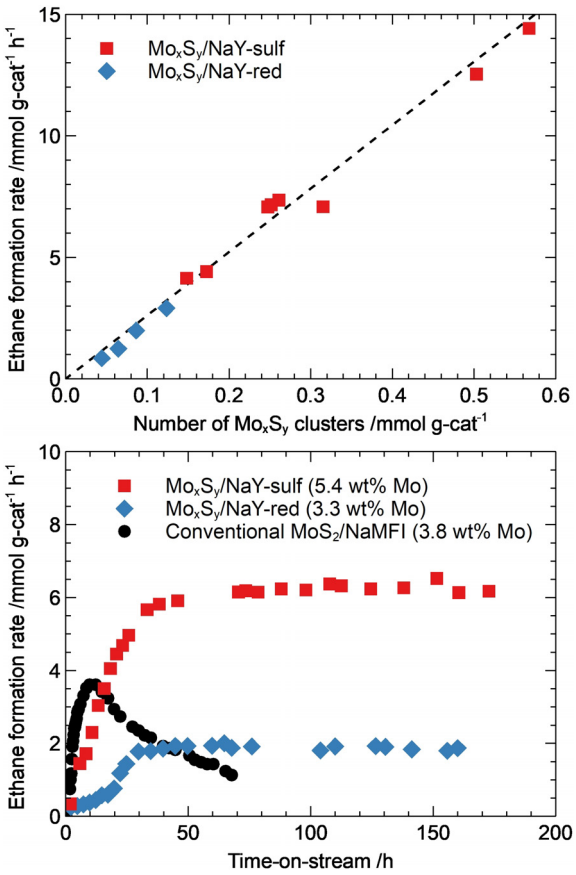

Figure 5. Steady-state ethane formation rates (top) at 473 K for cluster catalysts with different loadings and time-on-stream behavior (bottom) of representative Mo_xS_y/NaY-sulf/red catalysts and MoS_2/NaMFI.

Interestingly, when subjecting the two clusters catalysts to a stream of ethene and H_2, no activity was observed at the very beginning, but both catalysts gained activity and reached a steady-state over a time span of ≈30 h (Figure 5). Elemental analysis of the spent Mo_xS_y/NaY-sulf sample showed a loss of sulfur that corresponded to approximately one S per cluster. Thus, we hypothesize that partial sulfur loss from the fully sulfided Mo_2S_4 cluster may account for the generation of true active sites (S-vacancies) while the original clusters are inactive. Given the high reduction temperature (673 K in pure H_2), further reduction and sulfur loss is rather unlikely for the Mo_xS_y/NaY-red sample at the reaction temperature of 473 K and the induction period could be caused by restructuring.

While it would also be very important to understand a potential response of the Mo spin states to its local coordination environment, this is to be further investigated by in situ spectroscopy (EPR and XAS in particular) that monitors the dynamic evolution of the structure and chemical compositions of the active sites at reaction conditions.

For Mo_xS_y/NaY-sulf/red catalysts, a linear increase of the steady-state ethane formation rate (per gram of catalyst) was observed with an increasing loading of clusters (Figure 5). The parent NaY zeolite itself (no EFAl species or Brønsted acid sites; Figures S1 and S11) did not exhibit hydrogenation activity. Therefore, we conclude that the measured activity stems solely from Mo_xS_y clusters that are homogeneous in nature. Surprisingly, the linear rate increase was identical for di- and tetramers indicating that each cluster forms the same number of equally active sites.

The cluster catalysts showed stable steady-state conversion rates (for at least 7 days), allowing to conclude that the active sulfide sites hosted in the zeolite cages remained stable, in contrast to previous studies that either lacked evaluation of the stability metric or clearly noted deactivation/degradation of the active structures.[7a,b,8] A traditional MoS_2/NaMFI catalyst that featured extended slabs, however, deactivated markedly after reaching the maximum activity (Figure 5). The NaMFI zeolite used as a support is free of Brønsted acid sites and did not show any activity under the probed conditions. We, therefore, conclude that deactivation results from degradation of the MoS_2 phase without supply of sulfur in the reactant stream.

In summary, we have shown that di- and tetrameric Mo_xS_y clusters can be stabilized in a homogeneous form by zeolite Na-FAU. The active clusters are homogeneously distributed in the zeolite and are essentially homotopic. The specific catalytic activity of these clusters for ethene hydrogenation is identical. The tetrameric cluster is structurally similar to the Mo site of the FeMo-cofactor in nitrogenase. DFT-based optimization of the cluster geometry and free energy calculations predict that both clusters contain a single unpaired electron at each Mo atom. While the intrinsic catalytic activity is similar to those of a conventional supported MoS_2 catalyst, the latter deactivates markedly during time on stream while both the di-and tetrameric Mo_xS_y cluster-based catalysts are stable for days of operation. Thus, the zeolite-supported Mo_xS_y cluster catalysts are a promising new class of robust, bio-inspired hydrogenation catalysts that create exciting opportunities with respect to chemical and structural variability for catalysis.

Acknowledgements

This work was funded by the Chevron Energy Technology Company. The authors especially thank Dr. A. Kuperman and Dr. A. Brait (Chevron), and Prof. Takeshi Kubota (Shimane University, Japan) for fruitful discussions. Conceptual work and structural determinations were supported by the U.S. Department of Energy (DOE), Office of Science, Office of Basic Energy Sciences (BES), Division of Chemical Sciences, Geosciences and Biosciences (Transdisciplinary Approaches to Realize Novel Catalytic Pathways to Energy Carriers, FWP 47319). Portions of the experiments were performed at the William R. Environmental Molecular Science Laboratory (EMSL), a national scientific user facility sponsored by the DOE Office of Biological and Environmental Research located at Pacific Northwest National Laboratory (PNNL). PNNL is a multiprogram national laboratory operated for DOE by Battelle. The authors gratefully acknowledge the Leibniz Supercomputing Center for funding this project by providing computing time on their Linux-Cluster. The X-ray absorption and emission spectroscopy measurements were performed on beamline ID26 at the European Synchrotron Radiation Facility (ESRF), Grenoble, France (Proposal CH-

5641). We are grateful to Dr. Pieter Glatzel at the ESRF for his assistance. The authors also want to thank Dr. O. Storcheva (EPR spectroscopy), T. Schachtl and M. Aigner (NMR spectroscopy), and C. Gross (syntheses and reactions) for their help. Open access funding enabled and organized by Projekt DEAL.

Conflict of interest

The authors declare no conflict of interest.

Keywords: EPR spectroscopy · hydrogenation · molybdenum sulfide clusters · transition metal sulfides · zeolites

[1] a) J. B. Howard, D. C. Rees, *Chem. Rev.* **1996**, *96*, 2965 – 2982; b) B. K. Burgess, D. J. Lowe, *Chem. Rev.* **1996**, *96*, 2983 – 3011; c) J. Kowalska, S. DeBeer, *Biochim. Biophys. Acta Mol. Cell Res.* **2015**, *1853*, 1406 – 1415; d) K. M. Lancaster, M. Roemelt, P. Ettenhuber, Y. Hu, M. W. Ribbe, F. Neese, U. Bergmann, S. DeBeer, *Science* **2011**, *334*, 974 – 977; e) R. Bjornsson, F. Neese, R. R. Schrock, O. Einsle, S. DeBeer, *J. Biol. Inorg. Chem.* **2015**, *20*, 447 – 460; f) R. Bjornsson, F. A. Lima, T. Spatzal, T. Weyhermüller, P. Glatzel, E. Bill, O. Einsle, F. Neese, S. DeBeer, *Chem. Sci.* **2014**, *5*, 3096 – 3103; g) O. Einsle, F. A. Tezcan, S. L. A. Andrade, B. Schmid, M. Yoshida, J. B. Howard, D. C. Rees, *Science* **2002**, *297*, 1696 – 1700; h) S. J. George, B. M. Barney, D. Mitra, R. Y. Igarashi, Y. Guo, D. R. Dean, S. P. Cramer, L. C. Seefeldt, *J. Inorg. Biochem.* **2012**, *112*, 85 – 92; i) S. J. George, J. A. Hernandez, E. Jimenez-Vicente, C. Echavarri-Erasun, L. M. Rubio, *Chem. Commun.* **2016**, *52*, 11811 – 11814.

[2] a) M. Grilc, B. Likozar, J. Levec, *Appl. Catal. B* **2014**, *150 – 151*, 275 – 287; b) G. Liu, A. W. Robertson, M. M.-J. Li, W. C. H. Kuo, M. T. Darby, M. H. Muhieddine, Y.-C. Lin, K. Suenaga, M. Stamatakis, J. H. Warner, S. C. E. Tsang, *Nat. Chem.* **2017**, *9*, 810 – 816; c) S. Eijsbouts, S. W. Mayo, K. Fujita, *Appl. Catal. A* **2007**, *322*, 58 – 66.

[3] a) P. D. Tran, M. Nguyen, S. S. Pramana, A. Bhattacharjee, S. Y. Chiam, J. Fize, M. J. Field, V. Artero, L. H. Wong, J. Loo, J. Barber, *Energy Environ. Sci.* **2012**, *5*, 8912; b) P. D. Tran, T. V. Tran, M. Orio, S. Torelli, Q. D. Truong, K. Nayuki, Y. Sasaki, S. Y. Chiam, R. Yi, I. Honma, J. Barber, V. Artero, *Nat. Mater.* **2016**, *15*, 640 – 646; c) A.-Y. Lu, X. Yang, C.-C. Tseng, S. Min, S.-H. Lin, C.-L. Hsu, H. Li, H. Idriss, J.-L. Kuo, K.-W. Huang, L.-J. Li, *Small* **2016**, *12*, 5530 – 5537; d) D. Voiry, R. Fullon, J. Yang, C. de Carvalho Castro e Silva, R. Kappera, I. Bozkurt, D. Kaplan, M. J. Lagos, P. E. Batson, G. Gupta, A. D. Mohite, L. Dong, D. Er, V. B. Shenoy, T. Asefa, M. Chhowalla, *Nat. Mater.* **2016**, *15*, 1003 – 1009; e) B. Seo, S. H. Joo, *Nano Convergence* **2017**, *4*, 19.

[4] a) S. Helveg, J. V. Lauritsen, E. Laegsgaard, I. Stensgaard, J. K. Norskov, B. S. Clausen, H. Topsoe, F. Besenbacher, *Phys. Rev. Lett.* **2000**, *84*, 951 – 954; b) N.-Y. Topsoe, H. Topsoe, *J. Catal.* **1983**, *84*, 386 – 401.

[5] a) T. E. Wolff, J. M. Berg, K. O. H. Warrick, R. H. Holm, *J. Am. Chem. Soc.* **1978**, *100*, 4630 – 4632; b) H. Seino, M. Hidai, *Chem. Sci.* **2011**, *2*, 847.

[6] a) D. Coucouvanis, K. D. Demadis, S. M. Malinak, P. E. Mosier, M. A. Tyson, L. J. Laughlin, *J. Mol. Catal. A* **1996**, *107*, 123 – 135; b) D. Coucouvanis, P. E. Mosier, K. D. Demadis, S. Patton, S. M. Malinak, C. G. Kim, M. A. Tyson, *J. Am. Chem. Soc.* **1993**, *115*, 12193 – 12194; c) K. D. Demadis, S. M. Malinak, D. Coucouvanis, *Inorg. Chem.* **1996**, *35*, 4038 – 4046; d) S. M. Malinak, A. M. Simeonov, P. E. Mosier, C. E. McKenna, D. Coucouvanis, *J. Am. Chem. Soc.* **1997**, *119*, 1662 – 1667; e) K. Herbst, M. Monari, M. Brorson, *Inorg. Chem.* **2002**, *41*, 1336 – 1338; f) L. J. Laughlin, D. Coucouvanis, *J. Am. Chem. Soc.* **1995**, *117*, 3118 – 3125.

[7] a) M. Taniguchi, D. Imamura, H. Ishige, Y. Ishii, T. Murata, M. Hidai, T. Tatsumi, *J. Catal.* **1999**, *187*, 139 – 150; b) C.-E. Hédoire, E. Cadot, F. Villain, A. Davidson, C. Louis, M. Breysse, *Appl. Catal. A* **2006**, *306*, 165 – 174; c) A. Müller, S. Sarkar, R. G. Bhattacharyya, S. Pohl, M. Dartmann, *Angew. Chem. Int. Ed. Engl.* **1978**, *17*, 535; *Angew. Chem.* **1978**, *90*, 567; d) T. Shibahara, M. Yamasaki, G. Sakane, K. Minami, T. Yabuki, A. Ichimura, *Inorg. Chem.* **1992**, *31*, 640 – 647.

[8] E. J. M. Hensen, J. A. R. van Veen, *Catal. Today* **2003**, *86*, 87 – 109.

[9] a) T. Kadono, H. Chatani, T. Kubota, Y. Okamoto, *Microporous Mesoporous Mater.* **2007**, *101*, 191 – 199; b) T. Kadono, T. Kubota, H. Chatani, T. Kawabata, Y. Okamoto, *Stud. Surf. Sci. Catal.* **2006**, *162*, 849 – 856; c) Y. Okamoto, *Bull. Chem. Soc. Jpn.* **2014**, *87*, 20 – 58.

[10] a) Y. Okamoto, H. Katsuyama, K. Yoshida, K. Nakai, M. Matsuo, Y. Sakamoto, J. Yu, O. Terasaki, *J. Chem. Soc. Faraday Trans.* **1996**, *92*, 4647 – 4656; b) T. M. Salama, I. Othman, M. Sirag, G. A. El-Shobaky, *Microporous Mesoporous Mater.* **2006**, *95*, 312 – 320.

[11] a) C. Van Stappen, L. Decamps, G. E. Cutsail III, R. Bjornsson, J. T. Henthorn, J. A. Birrell, S. DeBeer, *Chem. Rev.* **2020**, *120*, 5005 – 5081; b) F. Biaso, B. Burlat, B. Guigliarelli, *Inorg. Chem.* **2012**, *51*, 3409 – 3419; c) C. J. Casewit, M. R. DuBois, *Inorg. Chem.* **1986**, *25*, 74 – 80.

Manuscript received: November 26, 2020
Revised manuscript received: February 5, 2021
Accepted manuscript online: February 11, 2021
Version of record online: March 17, 2021

